arXiv:cond-mat/0212401v1 [cond-mat.mtrl-sci] 17 Dec 2002

# FP-LMTO studies of hypothetical compounds with the $\beta$-SiAlON-like structure in Si–(Mg,Al)–O–N systems

S.V. Okatov*
*Institute of Solid State Chemistry, Ural Branch of the Russian Academy of Sciences, Pervomayskaya st., GSP-145, 620219, Ekaterinburg, Russia*
(Dated: February 1, 2008)

The electronic and energy properties of $\beta$-$Si_3N_4$ (a), $Si_{6-x}Al_xO_xN_{8-x}$ (b) and the hypothetical ordered solid solutions $Si_{6-x}Mg_xO_{2x}N_{8-2x}$ (c), $Si_{6-x}Mg_xO_xN_{8-2x}S_x$ (d), $Si_{6-x}Mg_xO_xN_{8-x}$ (e), $Si_{6-x}Mg_{x/2}Al_{x/2}O_xN_{8-x}$ (f) are considered by the *ab-initio* band FP-LMTO method. The calculations show that the stability of the systems decreases in the order: (a) > (b) > (f) > (e) > (c) > (d). It is established that $Si_{6-x}Mg_xO_xN_{8-x}$ and $Si_{6-x}Mg_{x/2}Al_{x/2}O_xN_{8-x}$ possess non-zero values of the density of states at the Fermi energy, which consists mainly of localized O2$p$, N2$p$ states, and the conductivity in those solid solutions is unlikely. It is found that the energy of the O2$s,p$ states tends to shift depending on the coordination environment of oxygen atoms in the considered systems. The energy of ordering of Al and Mg atoms in $Si_{6-x}Mg_{x/2}Al_{x/2}O_xN_{8-x}$ is estimated to be 3.15 eV/56-atomic supercell.

Keywords: Solid solutions, atomic ordering effects, bond indices, sialon, $\beta$-$Si_3N_4$, oxides, impurity channel

## I. INTRODUCTION

$\beta$-SiAlONs are solid solutions (SS) of variable composition formed from $\beta$-$Si_3N_4$ by Al → Si, O → N substitutions (composition $Si_{6-x}Al_xO_xN_{8-x}$, $x = 0 - 4.2$). They possess a unique set of high thermal and chemical stability, hardness, thermal conductivity, electroinsulating characteristics, which define their application in ceramic industry [1]. Some peculiarities of the electronic structure of these disordered SS are considered in papers [2, 3, 4].

The investigation of atomic ordering effects (AOE) [5] by the semi-empirical tight-binding band method (EHT) allowed to predict the existence of the so-called "impurity channels" in $\beta$-SiAlON — extended along $c$ axis quasi-one-dimensional (1D) structures constituted by 12-atomic alumoxide rings (fig. 1). The simulation of the ordered and disordered states of $\beta$-SiAlON by the cluster discrete variation method (DVM) [6] and the band full-potential linear muffin-tin orbitals method (FP-LMTO) [7] confirmed higher stability of the ordered state and revealed differences in their electronic structure and bond indices.

The formation of 1D-structures in $\beta$-SiAlON was explained in [5] by the "trend" of the system to reduce the number of Si–O, Al–O bonds containing unfavorable antibonding states. This resulted in localization of those states in impurity channels. Taking this fact into account, it was supposed in [8] that the reduction of valence electrons concentration (VEC) in the impurity channels by the partial substitution Al → $M^{I,II}$ ($M^{I,II}$ — I, II group elements, composition $Si_{6-x}Al_{x-y}M^{I,II}{}_yO_xN_{8-x}$) might increase the stability of the material and induce the conductivity, which would be localized in 1D-structures.

Further investigations of AOE in the Si–Mg–O–N system by the EHT method [9] showed that SS of the $Si_{6-x}Mg_xO_{2x}N_{8-2x}$ composition could not be formed because of unlimited growth of clusters containing Mg and O atoms. That result was supported by experiments [10, 11]. According to [9], the stabilization of SS in the Si–Mg–O–N system was possible at the stoichiometric compositions $Si_{6-x}Mg_xO_xN_{8-x}$ or with stabilizing additives, for example Zr ($Si_{6-x}Mg_{x/2}Zr_{x/2}O_xN_{8-x}$) or S ($Si_{6-x}Mg_xO_xN_{8-2x}S_x$). For the latter system, antibonding impurity states were found in the bandgap interval of $Si_3N_4$, which meant a low stability of such SS. Analogous data were obtained for the Si–Be–O–N system [12].

In this paper, the electronic and energy properties of $\beta$-$Si_3N_4$, $Si_{6-x}Al_xO_xN_{8-x}$, as well as potentially stable structures $Si_{6-x}Mg_xO_{2x}N_{8-2x}$, $Si_{6-x}Mg_xO_xN_{8-2x}S_x$, $Si_{6-x}Mg_xO_xN_{8-x}$, $Si_{6-x}Mg_{x/2}Al_{x/2}O_xN_{8-x}$ obtained in [9], are simulated by the *ab-initio* FP-LMTO method.

## II. METHODS AND MODELS

The basic $\beta$-$Si_3N_4$ has a hexagonal structure with the $P6_3$ space group, lattice constants $a = 7.586$, $c = 2.902$Å and contains 14 atoms in a unit cell [13]. In the present calculations, we used 56-atomic supercells ($2\times2\times1$) similar to those applied in [7]. The following compositions of the supercells are considered: $Si_{24}N_{32}$, $Si_{18}Al_6O_6N_{26}$, $Si_{18}Mg_6O_{12}N_{20}$, $Si_{18}Mg_6O_6N_{20}S_6$, $Si_{18}Mg_6O_6N_{26}$, $Si_{18}Mg_3Al_3O_6N_{26}$, which correspond to the stoichiometric compositions $Si_3N_4$, $Si_{6-x}Al_xO_xN_{8-x}$, $Si_{6-x}Mg_xO_{2x}N_{8-2x}$, $Si_{6-x}Mg_xO_xN_{8-2x}S_x$, $Si_{6-x}Mg_xO_xN_{8-x}$, $Si_{6-x}Mg_{x/2}Al_{x/2}O_xN_{8-x}$ ($x = 1.5$, fig. 1), respectively. The atoms distribution in the cells complies with [5, 9], the lattice relaxation is not taken into account. For the $Si_{6-x}Mg_xO_{2x}N_{8-2x}$ and $Si_{6-x}Mg_xO_xN_{8-2x}S_x$ SS, N1 atoms are replaced respectively by O and S atoms (fig. 1a), which are in

*okatov@ihim.uran.ru

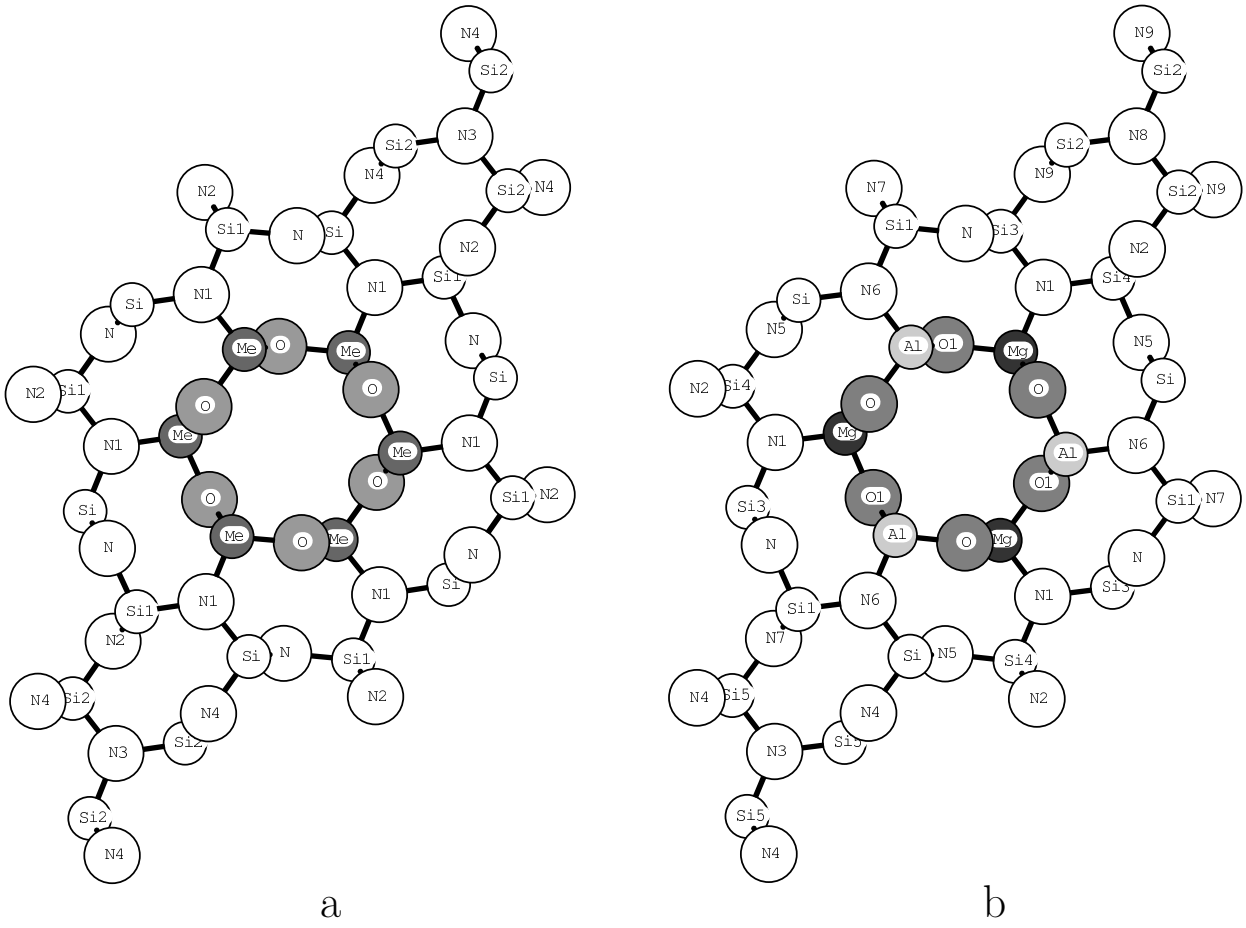


FIG. 1: Models of the ordered $Si_{6-x}Me_xO_xN_{8-x}$ (a, Me = Al, Mg) and $Si_{6-x}Mg_{x/2}Al_{x/2}O_xN_{8-x}$ (b) structures containing impurity channels. Si–Si5, N–N9 — nonequivalent positions of Si and N, respectively.

"excess" in comparison with $Si_{6-x}Al_xO_xN_{8-x}$, see [9].

The calculations are performed in the framework of the local density approximation (LDA) by the FP-LMTO method [14]. The realization of this method differs from that in [7] by using smoothed Hankel functions instead of unsmoothed ones, and by the representation of the charge density. In [7], it was defined as $n = n_{\rm MT} + n_{rem}$, where $n_{\rm MT}$, $n_{rem}$ — densities within and outside the spheres, respectively, while in [14] it is expressed as $n = n_0 + n_1 - n_2$, where $n_0$–$n_2$ are respectively a smooth density carried on a uniform mesh, the true density in a $Y_L$ expansion inside each augmentation sphere, and a one-center expansion of the smooth density inside each augmentation sphere.

The correlation energy in this work is calculated with the Barth-Hedin formula [15]. As $a/c, b/c \sim 0.2 \ll 1$ for the chosen supercells, the $8\times8\times40$ and $54\times54\times9$ meshes are used for the $k$-space and charge density, respectively. To satisfy the method's requirement of close-packing, 48 "empty" spheres are included. The following values of sphere radii are chosen: 1.75 (Si, Al, Mg), 1.47 (N, O, S) and 1.51–2.05 a.u. (for empty spheres). The atomic orbital basis set includes $s, p, d$ states for Mg, Al, Si; $s, p$ electrons for N, O, S; and $s$ states for empty spheres.

## III. RESULTS AND DISCUSSION

### A. $\beta$-$Si_3N_4$ and $Si_{6-x}Al_xO_xN_{8-x}$

The electronic properties of $Si_3N_4$ and $Si_{6-x}Al_xO_xN_{8-x}$ are considered in [2, 6, 7, 16, 17, 18] in detail. Here we discuss only the differences in the electronic and energy characteristics of the ordered systems, which are due to the method [14] applied.

The band structures (BS) and the total densities of states (TDOS) of $\beta$-$Si_3N_4$ and $Si_{6-x}Al_xO_xN_{8-x}$ are depicted in fig. 2a,b. Their band parameters and cohesion energies ($E_{coh}$) are presented in table I in comparison with the data of other publications. In good agreement with [6, 7, 16, 17, 18], the valence band (VB) of $\beta$-$Si_3N_4$ contains two subbands (SB) — a low SB consisting of N2$s$

TABLE I: Bandgaps, valence band subbands (SB), forbidden states intervals (FSI) widths (eV, fig. 2) and cohesion energies (eV/atom) of $\beta$-$Si_3N_4$ and $Si_{6-x}Al_xO_xN_{8-x}$ obtained in these calculations and taken from other publications.

| Parameter | these results | [7][a] | [6][b] | [16] | [17] | [18] | Exp. [19, 20, 21, 22] |
|---|---|---|---|---|---|---|---|
| **$Si_3N_4$** | | | | | | | |
| $\Delta E_g$ | 4.4 | 4.1 | 5.1 | 4.2 | 4.96 | 5.18 | 4.6-5.5 |
| SB (high) | 10.7 | 10.0 | ∼11 | 10.1 | 9.79 | 8.91 | — |
| FSI | 5.1 | 4.3 | ∼3 | 3.9 | — | 4.19 | — |
| SB (low) | 3.7 | 4.0 | ∼5 | 4.2 | 4.12 | 3.49 | — |
| $E_{coh}$ | 5.18 | 6.71 | — | 5.31 | — | — | 5.93 |
| **$Si_{6-x}Al_xO_xN_{8-x}$** | | | | | | | |
| $\Delta E_g$ | 1.9 | 2.2 | 4.0 | | | | |
| SB (high) | 12.2 | 9.9 | ∼11 | | | | |
| FSI (high) | 3.4 | 4.1 | ∼3 | | | | |
| SB (middle) | 3.7 | 4.0 | ∼5 | | | | |
| FSI (low) | 5.4 | 2.5 | ∼1 | | | | |
| SB (low) | 1.1 | 1.4 | ∼2 | | | | |
| $E_{coh}$ | 4.43 | 6.23 | — | | | | |

[a] The methods used: [7] — FP-LMTO, [6] — DVM, [16] — pseudopotential, [17] — OLCAO, [18] — LMTO-ASA

[b] The presented parameters correspond to $Si_{6-x}Al_xO_xN_{8-x}$ with $x = 1$.

and Si3$s, p, d$ states and a high SB, which includes N2$p$ and Si3$s, p, d$ states and separated from the conduction band (CB) by a wide bandgap ($\Delta E_g = 4.4$ eV). It is seen that, according to various authors [6, 7, 16, 17, 18], the bandgap width of $Si_3N_4$ ranges from 4.1 to 5.18 eV, thus, our result agrees well with the above findings. This value is smaller than the experimental one, but it is a characteristic feature of the LMTO methods. A similar degree of agreement can be found for other band parameters (see table I) except for a wider forbidden states interval (FSI). The positions, intensities and compositions of the main peaks in this calculation are also in agreement corresponding to that of the above parameters. Our $E_{coh}$ value (5.18) also compies well with that obtained in [16] (5.31 eV/atom), but differs essentially from that in [7]. A value closer to the latter result is obtained if we choose a thin $30 \times 30 \times 6$ direct space mesh. Our calculations of $\beta$-$Si_3N_4$ with a 14-atomic cell and a denser mesh yield $E_{coh} = 5.27$ eV/atom.

$\beta$-SiAlON contains three SB in the VB — high (O2$s$, N2$s$, Si3$s, p, d$, Al3$s, p, d$), middle (N2$s$, Si3$s, p, d$ and a small amount of Al3$s, p, d$) and low (O2$s$, Al3$s, p, d$) — separated from each other by two forbidden states intervals (FSI), fig. 2b. Its bandgap ($\Delta E_g = 1.9$ eV), SB, FSI widths and the cohesion energy ($E_{coh} = 4.43$ eV/atom) (table I) agree with the data of other pulications [6, 7] as they did for $Si_3N_4$ above.

Generally, the present results are in good agreement with other calculations and experiments.

TABLE II: The bandgap widths ($\Delta E_g$), population at the Fermi energy ($N(E_F)$) and cohesion energies ($E_{coh}$) of the systems considered.

| Composition | $\Delta E_g$, eV | $N(E_F) \cdot 10^{-3}$, states/eV cell | $E_{coh}$, eV/atom |
|---|---|---|---|
| $Si_3N_4$ | 4.4 | 0 | 5.18 |
| $Si_{6-x}Al_xO_xN_{8-x}$ | 1.9 | 0 | 4.43 |
| $Si_{6-x}Mg_xO_{2x}N_{8-2x}$ | 0 | 0 | 3.20 |
| $Si_{6-x}Mg_xO_xN_{8-2x}S_x$ | 1.6 | 0 | 3.00 |
| $Si_{6-x}Mg_xO_xN_{8-x}$ | 0 | 3.0 | 3.80 |
| $Si_{6-x}Mg_{x/2}Al_{x/2}O_xN_{8-x}$ | 0 | 2.0 | 4.17 |

### B. $Si_{6-x}Mg_xO_{2x}N_{8-2x}$

According to [9], the structure of the $Si_{6-x}Mg_xO_{2x}N_{8-2x}$ SS used in this calculation (fig. 1) is not the only possible one. This configuration is chosen because its symmetry coincides with that of $Si_{6-x}Al_xO_xN_{8-x}$, which allows to consider only the chemical composition altering effects without the symmetry correction.

The band structure and TDOS of the $Si_{6-x}Mg_xO_{2x}N_{8-2x}$ SS are shown in fig. 2c and some band and energy parameters are listed in table II. One can see that the system contains Mg3$s, p, d$, Si3$s, p, d$, N2$p$, O2$p$ states in the bandgap interval of $Si_3N_4$ and is a semimetal with $\Delta - \Gamma$ transition. The presence of those states causes a shift of the spectrum of the system by $\sim 4$ eV downwards as compared with $Si_3N_4$. The TDOS of $Si_{6-x}Mg_xO_{2x}N_{8-2x}$ contains also two quasi-core SB of O2$s$ states. The lower one (A, fig. 2) looks like that in $\beta$-SiAlON, whereas the higher SB (B) is specific for this SS.

The cohesion energy of the $Si_{6-x}Mg_xO_{2x}N_{8-2x}$ SS is 3.2 eV/atom, which is much less than that for $\beta$-SiAlON and especially for $\beta$-$Si_3N_4$. This fact confirms the conclusion [9] about instability of the $Si_{6-x}Mg_xO_{2x}N_{8-2x}$ SS.

### C. $Si_{6-x}Mg_xO_xN_{8-2x}S_x$

According to [9], the presence of sulfur in $Si_{6-x}Mg_xO_xN_{8-2x}S_x$ leads to appearance of filled states in the bandgap interval, which includes antibonding states of Si–N, Si–S bonds. Let us compare that model with *ab-initio* calculations results.

As is seen from (fig. 2d), the TDOS of $Si_{6-x}Mg_xO_xN_{8-2x}S_x$ contains the impurity states separated into a subband C composed by Si3$s, p, d$, S2$p$, N2$p$ states and admixed to the lower edge of the CB. This results in almost tree-times reduction of the bandgap width ($\Delta E_g = 1.6$ eV, table II) with respect to $\beta$-$Si_3N_4$. The bandgap in $Si_{6-x}Mg_xO_xN_{8-2x}S_x$ is formed by the indirect transition $\Delta_1 - \Delta_2$. Another subband D of O2$s$ states appears near the N2$s$ subband. The S2$s$ and S2$p$ states are admixed to the N2$s$ and N2$p$ SB.

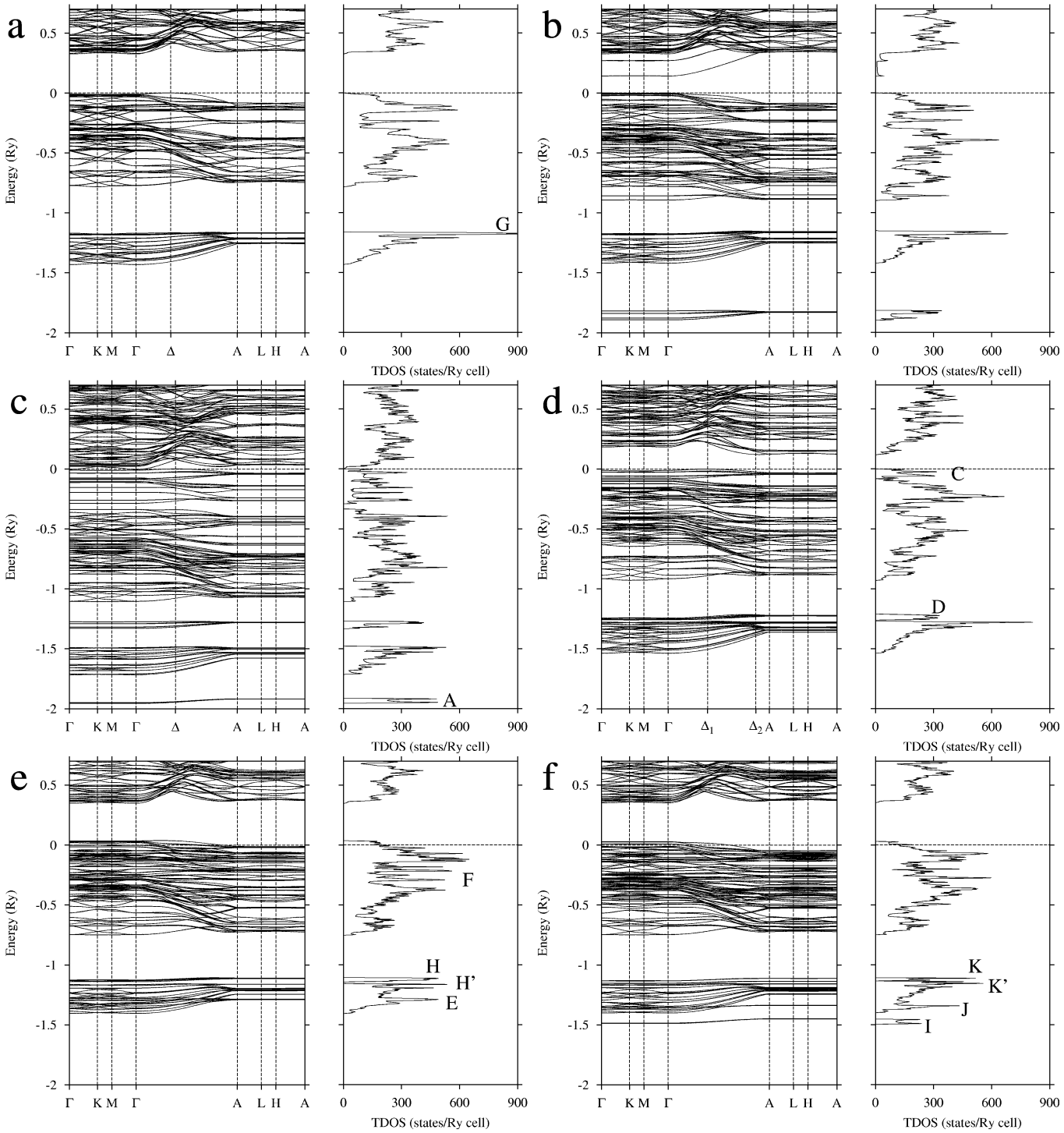


FIG. 2: The band structure (*left panels*) and the total densities of states (*right*) of $\beta$-$Si_3N_4$ (a), $Si_{6-x}Al_xO_xN_{8-x}$ (b) and hypothetical ordered solid solutions $Si_{6-x}Mg_xO_{2x}N_{8-2x}$ (c), $Si_{6-x}Mg_xO_xN_{8-2x}S_x$ (d), $Si_{6-x}Mg_xO_xN_{8-x}$ (e), $Si_{6-x}Mg_{x/2}Al_{x/2}O_xN_{8-x}$ (f).

In agreement with [9], the cohesion energy of $Si_{6-x}Mg_xO_xN_{8-2x}S_x$ is 3.0 eV/atom, which indicates a low stability of such SS.

### D. $\mathbf{Si_{6-x}Mg_xO_xN_{8-x}}$

The band structure and TDOS of $Si_{6-x}Mg_xO_xN_{8-x}$ are depicted in fig. 2e. The partial densities of states (PDOS) are also shown in fig. 3. It is seen that the

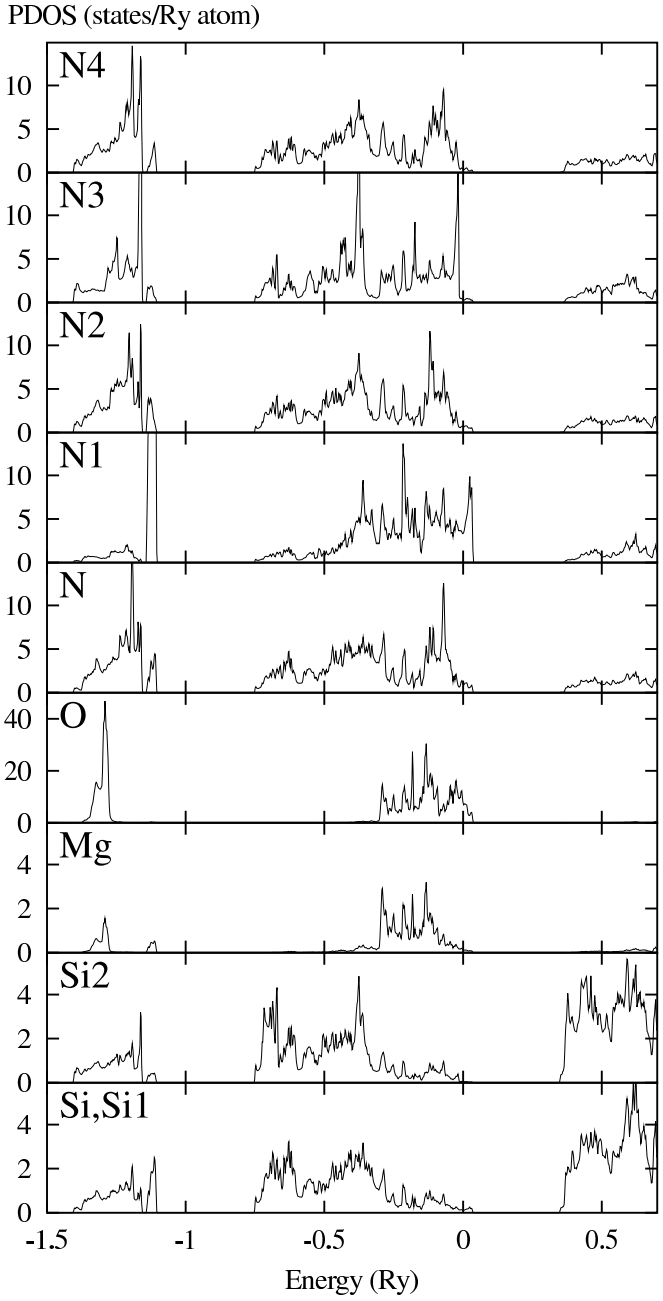


FIG. 3: The partial densities of states of $Si_{6-x}Mg_xO_xN_{8-x}$. Si–Si2, N–N4 — nonequivalent positions of Si, N atoms (fig. 1a).

TDOS of $Si_{6-x}Mg_xO_xN_{8-x}$ contains two subbands in the VB — high and low — with contributions from Si3$s,p,d$, N2$p$, Mg3$s,p,d$, O2$p$ and Si3$s,p,d$, N2$s$, Mg3$s,p,d$, O2$s$ states respectively. The substitution Mg → Al in $Si_{6-x}Al_xO_xN_{8-x}$ leads to electron deficiency in the resulting $Si_{6-x}Mg_xO_xN_{8-x}$. Thus, this brings about a shift of the Fermi energy ($E_F$) to a lower value and gives rise to electronic states at $E_F$, the number of which is $N(E_F) = 3.0 \cdot 10^3$ states/eV cell (table II).

The lower edge of the CB of $Si_{6-x}Mg_xO_xN_{8-x}$ is formed mainly by O2$p$ and to a lesser degree by N2$p$ states. Their contributions to the density of states at the Fermi energy ($N_i(E_F)$, i=Si–Si3, N–N4, Mg, O) are 101 (O), 46 (N1), 12 (N), 8 (N2), 5 (N4), 4 (N3) states/eV atom in the order of distances from the impurity channel (fig. 1). Other atoms do not give any substantial number of states to $N(E_F)$: 1.4 (Mg, Si, Si1), 0.5 (Si2) states/eV atom. This is indicative of a localized character of free O- and N-states, hence, we do not expect electroconductivity in $Si_{6-x}Mg_xO_xN_{8-x}$. A decrease in the atoms contribution to $N(E_F)$ with the distance from the impurity channel demonstrates the charge screening effect.

As is seen from PDOS (fig. 3), Mg- and O-states are concentrated mainly in $[-1.4 : -1.2]$ (O2$s$, Mg3$s$) and $[-0.4 : 0.05]$ Ry (O2$p$, Mg3$s,p,d$) intervals (respectively, $[-19.0 : -16.3]$ and $[-5.4 : 0.7]$ eV). The lower Mg–O hybridized states are responsible for formation of the E (fig. 2e) peak, whereas the higher states contribute into the F region. The degenerated Si3$p$-N2$s$ states of the highest peak (G, fig. 2a) of the lower subband in $Si_3N_4$ are split into H and H' peaks (fig. 2e) in $Si_{6-x}Mg_xO_xN_{8-x}$. This is due to the charge nonequivalence of Si–Si2 and N–N4 atoms (fig. 1). The greatest contribution to the H peak is made by N1 atoms; it decreases with the distance from the impurity channel (fig. 3). On the contrary, the contribution to the H' peak increases.

The cohesion energy calculation of $Si_{6-x}Mg_xO_xN_{8-x}$ (3.8 eV/atom) revealed a higher stability of this SS in comparison with the $Si_{6-x}Mg_xO_{2x}N_{8-2x}$ and $Si_{6-x}Mg_xO_xN_{8-2x}S_x$ systems (table II).

### E. SS of the general composition $Si_{6-x}Mg_{x-y}M_yO_xN_{8-x}$

As was noted above, O, N atoms have a large amount of states at $E_F$ in the $Si_{6-x}Mg_xO_xN_{8-x}$ SS, but the conductivity is unlikely in this SS mainly because of a low contribution of Mg atoms to $N(E_F)$. It may be supposed that the conductivity can be increased by partial substitution Mg→M (composition $Si_{6-x}Mg_{x-y}M_yO_xN_{8-x}$), which favors the formation of electronic states at $E_F$. In this case the conductivity along –M–O–M–O– chains can be expected. This means that, depending on the stacking type of M and Mg atoms, quasi-linear, ring-like or spiral conductors can be formed at $y = x/3 - x/2$, which are separated from each other by insulating –Mg–O–Mg–O– chains, fig. 4.

The most interesting case is that of spiral structures, which may be interpreted as nano-sized solenoids. A potential difference applied to that solenoid may induce the magnetic field localized within the impurity channel and directed along the $c$ axis. This effect can be used, in particular, for producing electronic memory. For instance, by placing the magnetic atoms into the cavity of the impurity channel and altering the juice direction, it may be possible to change the direction of their magnetic mo-

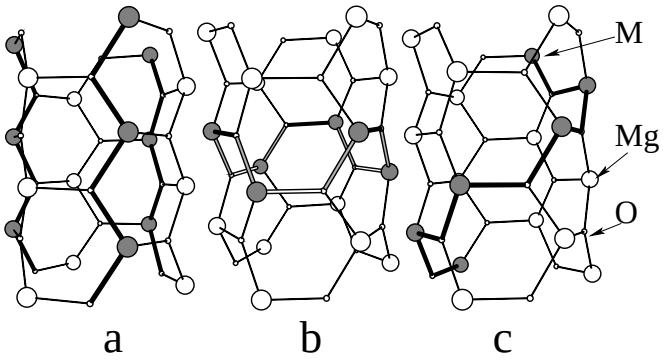


FIG. 4: Possible distributions of Mg and M atoms in $Si_{6-x}Mg_{x-y}M_yO_xN_{8-x}$ within the impurity channel: quasi-linear (a), ring-like (b) and spiral (c).

ments vectors. This may be interpreted as the changing of the memory element state ($0 \to 1$ or $1 \to 0$).

At present, the search for the compositions in the $Si_{6-x}Mg_{x-y}M_yO_xN_{8-x}$ systems is in progress.The $Si_{6-x}Mg_{x/2}Al_{x/2}O_xN_{8-x}$ SS is considered below as an example.

### F. $Si_{6-x}Mg_{x/2}Al_{x/2}O_xN_{8-x}$

In this paper we study the $Si_{6-x}Mg_{x/2}Al_{x/2}O_xN_{8-x}$ SS with the quasi-linear type of ordering of Al and Mg atoms (fig. 1b, 4a).

The substitution of Al atoms for Mg in $Si_{6-x}Mg_xO_xN_{8-x}$ causes the following changes in the electronic and energy properties (fig. 2f, table II) of the resulting $Si_{6-x}Mg_{x/2}Al_{x/2}O_xN_{8-x}$. Subband I of quasi-core O2$s$ states is formed, which is similar that in $Si_{6-x}Al_xO_xN_{8-x}$ one, but the first SB lies in a higher energy interval than the second one (fig. 2b,f). Pick J shifts by $\sim$ 0.7 eV downword with respect to peak E in $Si_{6-x}Mg_xO_xN_{8-x}$, and the distance between peaks K and K' shortens in comparison with H and H' (fig. 2e,f). The TDOS at $E_F$ decreases ($2.0 \cdot 10^3$ states/eV cell) in $Si_{6-x}Mg_{x/2}Al_{x/2}O_xN_{8-x}$ with respect to $Si_{6-x}Mg_xO_xN_{8-x}$ (table II), which is due to partial filling of empty O2$p$ states in $Si_{6-x}Mg_xO_xN_{8-x}$ occurring when Al atoms replace Mg. In general, the electronic structure of $Si_{6-x}Mg_{x/2}Al_{x/2}O_xN_{8-x}$ has an intermediate shape between $Si_{6-x}Al_xO_xN_{8-x}$ and $Si_{6-x}Mg_xO_xN_{8-x}$, but the splitting of O2$s,p$ states, which occurs in $\beta$-SiAlON when high symmetry structures (impurity channels) are formed, is not observed.

The analysis of PDOS (fig. 5) shows that peaks I, J (fig. 2) are constituted by O2$s$ states of O1 and O atoms respectively. Taking into account the difference in the environment of O and O1 atoms ($OAlMg_2$, $O1Al_2Mg$), one can trace the tendency of shifting O2$s$ states with increasing amount of Al in the coordination of O-atoms. The positions of the highest peaks in O2$s$ subbands for the $OAl_3$, $OAl_2Mg$, $OAlMg_2$, $OMg_3$ coordinations are $-1.818$, $-1.45$, $-1.34$, $-1.29$ Ry ($-24.74$, $-19.73$, $-18.23$, $-17.55$ eV), respectively (see fig. 2, 3, 5). A similar tendency can be determined also for O2$p$ states.

According to fig. 5, the closest to Mg atoms N1, N, N2 and Si3, Si4, Si2 (in the order of distances from Mg) are responsible for the splitting of N2$s$ states into K and K' peaks, and their contribution into K peak grows with approaching to Mg.

In spite of a small change in the $N(E_F)$ value for $Si_{6-x}Mg_{x/2}Al_{x/2}O_xN_{8-x}$ in comparison with $Si_{6-x}Mg_xO_xN_{8-x}$, the composition of the TDOS at $E_F$ differs considerably. If in $Si_{6-x}Mg_xO_xN_{8-x}$ the highest value of $N_{\rm i}(E_F)$ belongs to i = O atoms, in the $Si_{6-x}Mg_{x/2}Al_{x/2}O_xN_{8-x}$ SS it is not so high (16, 5 states/eV atom for O, O1, respectively; fig. 5). The main contribution to $N(E_F)$ is made by N6 (95) and N1 (54 states/eV atom). The larger value of $N_{\rm N6}(E_F)$ occurs because the Fermi energy is at a peak for those atoms, whereas for N1 atoms it is on a slope. In the $Si_{6-x}Mg_{x/2}Al_{x/2}O_xN_{8-x}$ SS, $N_{\rm i}(E_F)$ tends to decrease with the distance from Mg atoms (54 (N1), 14 (N2), 11 (N, N9), 8 (N8); 1.4 (Si3, Si4), 0.7 (Si2)) similarly to that in $Si_{6-x}Mg_xO_xN_{8-x}$. But this cannot take place for the atoms closest to Al (95 (N6), 14 (N7), 16 (N5), 12 (N4), 19 (N3); 2.7 (Si, Si1), 0.7 (Si5)). The data presented here reveal a localized character of the free states. Therefore, we expect $Si_{6-x}Mg_{x/2}Al_{x/2}O_xN_{8-x}$ to be an insulator.

The cohesion energy of the $Si_{6-x}Mg_{x/2}Al_{x/2}O_xN_{8-x}$ SS is 4.17 eV/atom (table II). This value can be used for the analysis of ordering in the system in question. As the impurity channels in this system are at a considerable distance from each other, we may assume that the interaction between them is small. Hence, we admit that the cohesion energy of the system of the composition $Si_{6-x}Mg_{x/2}Al_{x/2}O_xN_{8-x}$, which includes separate Al- and Mg-containing impurity channels, is expressed by the formula $E_{coh}^{Sep} = 0.5 \cdot (E_{coh}^{\rm Si_{6-x}Al_xO_xN_{8-x}} + E_{coh}^{\rm Si_{6-x}Mg_xO_xN_{8-x}})$. Thus, the energy of ordering of Al and Mg atoms is $E_o = E_{coh}^{Sep} - E_{coh}^{\rm Si_{6-x}Mg_{x/2}Al_{x/2}O_xN_{8-x}} = 0.055$ eV/atom (3.15 eV/cell). This means that the ordering of Al and Mg atoms in the form of alternating quasi-linear chains (fig. 4a) is more favorable.

## Conclusions

The simulation of electronic and energy properties of $\beta$-$Si_3N_4$, $Si_{6-x}Al_xO_xN_{8-x}$ and hypothetical ordered $Si_{6-x}Mg_xO_{2x}N_{8-2x}$, $Si_{6-x}Mg_xO_xN_{8-2x}S_x$, $Si_{6-x}Mg_xO_xN_{8-x}$, $Si_{6-x}Mg_{x/2}Al_{x/2}O_xN_{8-x}$ SS allows to make the following conclusions.

1. Comparison of the present results with the data of other publications for $\beta$-$Si_3N_4$ and

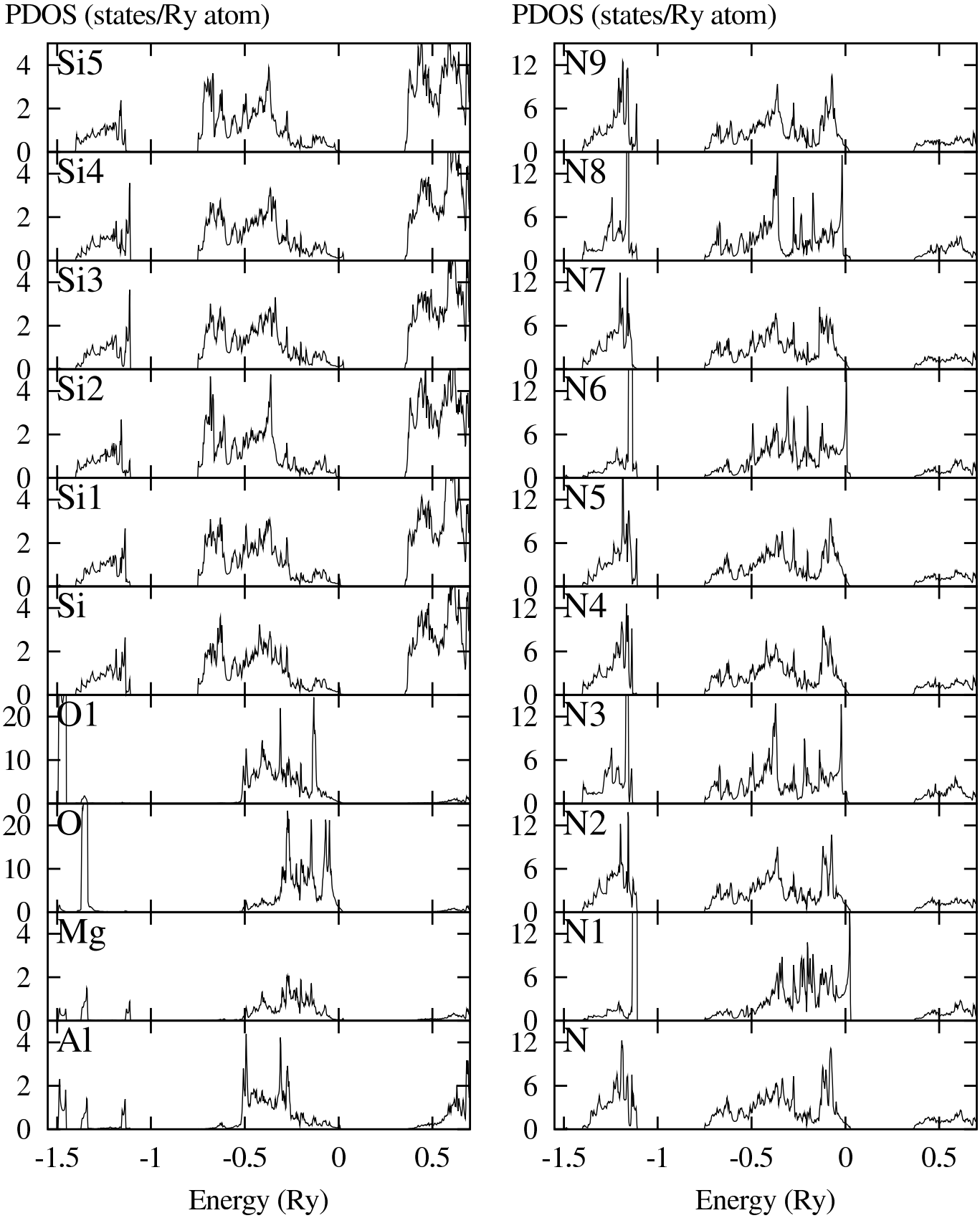


FIG. 5: The partial densities of states of $Si_{6-x}Mg_{x/2}Al_{x/2}O_xN_{8-x}$. Si–Si5, N–N9 — nonequivalent positions of atoms Si, N (fig. 1b).

$Si_{6-x}Al_xO_xN_{8-x}$ systems exhibits a good quality of the calculations performed.

2. The stability of the considered systems decrease in the following order: $Si_3N_4$ > $Si_{6-x}Al_xO_xN_{8-x}$ > $Si_{6-x}Mg_{x/2}Al_{x/2}O_xN_{8-x}$ > $Si_{6-x}Mg_xO_xN_{8-x}$ > $Si_{6-x}Mg_xO_{2x}N_{8-2x}$ > $Si_{6-x}Mg_xO_xN_{8-2x}S_x$. The low stability of $Si_{6-x}Mg_xO_{2x}N_{8-2x}$ and $Si_{6-x}Mg_xO_xN_{8-2x}S_x$ is in agreement with experimental data and earlier theoretical studies.

3. The density of states at the Fermi energy in $Si_{6-x}Mg_xO_xN_{8-x}$ is $3.0 \cdot 10^3$ states/eV cell, but it includes mainly localized O2$p$, N2$p$ states, and the conductivity in $Si_{6-x}Mg_xO_xN_{8-x}$ is unlikely.

4. Similarly to $Si_{6-x}Mg_xO_xN_{8-x}$, in the $Si_{6-x}Mg_{x/2}Al_{x/2}O_xN_{8-x}$ SS the number of states at $E_F$ is considerable ($2.0 \cdot 10^3$ states/eV cell), but they involve mainly localized N2$p$ and to a less degree O2$p$ states, so, the conductivity here is unlikely. It is established that the positions of O2$s, p$ states in $Si_{6-x}Mg_{x/2}Al_{x/2}O_xN_{8-x}$ strongly depend on the coordination environment of O atoms. Those states shift upward in the series $OAl_3$ →$OAl_2Mg$→$OAlMg_2$ →$OMg_3$. The energy of ordering of Al and Mg atoms is estimated to be 3.15 eV/cell.

5. Considering various distributions of M and Mg atoms in the SS of the general composition $Si_{6-x}Mg_{x-y}M_yO_xN_{8-x}$, we supposed the possibility of the formation of quasi-linear, ring-like and spiral conductors, which can be used, in particular, for quantum memory elements production. However, the simulation of the $Si_{6-x}Mg_{x/2}Al_{x/2}O_xN_{8-x}$ SS shows that it does not possess such properties. To find a particular composition of the $Si_{6-x}Mg_{x-y}M_yO_xN_{8-x}$ solid solution, we are going to study other possible alternatives (M = Sc, Ga, Y).

### Acknowledgments

This work was supported by the Russian Foundation for Basic Research, grant # 01-03-96515 (Ural).

[1] A.L. Ivanovskii // Russ. J. Inorg. Chem. **45**, Suppl. 1, 1 (2000).
[2] W.-Y. Ching, M.-Z. Huang, S.-D. Mo // J. Amer. Ceram. Soc. **83**, 780 (2000).
[3] I. Tanaka, S. Nasu, H. Adachi, Y. Miyamoto, K. Niihara //Acta Metal. Mater. **40**, 1995 (1992).
[4] I. Tanaka, K. Niihara, S. Nasu, H. Adachi // J. Amer. Ceram. Soc. **76**, 2883 (1995).
[5] S.V. Okatov, A.L. Ivanovskii // Int. J. Inorg. Mater. **3**, 923 (2001).
[6] M.V.Ryzhkov, A.L.Ivanonskii // J. Struct. Chem. **93**, 18 (2002).
[7] S.V.Okatov, A.L.Ivanovskii // phys. stat. sol. **B231**, R11 (2002).
[8] S.V. Okatov, PhD thesis "Electronic structure, chemical bonding and atomic ordering effects in oxynitride ceramics: Al–N–O, Si–Al–N–O and Zr–N–O systems". Ekaterinburg: 2001.
[9] S.V. Okatov, A.L. Ivanovskii // Refr. Indust. Ceram. (in press)
[10] Z. Zurek, J. Jedlinski, A. Gil, G. Borchardt // Mater. Sci. Forum. **251-2**, 877, Part 1-2 (1997).
[11] O. Yamamoto, M. Ishida, T. Sasamoto, S. Shimada // Int. J. Inorg. Mater. **3**, 715 (2001).
[12] S.V. Okatov // cond-mat/0212397
[13] R. Grün // Acta Cryst. **B35**, 800 (1979).
[14] M. Methfessel, Mark van Schilfgaarde, and R.A. Casali, "A full potential LMTO method based on smooth Hankel functions" in Electronic Structure and Physical Properties of Solids: The Uses of the LMTO Method, Lecture Notes in Physics **535**. H.Dreysse, ed. (Springer-Verlag, Berlin) 2000.
[15] U. von Barth and L. Hedin // J. Phys. C **5**, 1629 (1975).
[16] A.Y. Liu, M.L. Cohen // Phys. Rev. **B41**, 10727 (1990).
[17] Y.-U. Xu, W.-Y. Ching // Phys. Rev. **B51**, 17379 (1995).
[18] Y. Duan, K. Zhang, X. Xie // phys. status solidi. **B200** 499 (1997).
[19] Lange's Handbook of Chemistry. 12-th ed. Edited by J.A. Dean. New York: McGraw Hill. 1979.
[20] R.D. Carson, S.E. Schnatterly // Phys. Rev. **B33**, 2432 (1986).
[21] A.L. Shabalov, M.S. Feldman, M.Z. Bashirov // phys. stat. solidi **B145**, K71 (1988).
[22] C. Sénémaud, M. Driss-Khodja, A. Gheorghiu, S. Harel, G. Dufour, H. Roulet // J. Appl. Phys. **74**, 5042 (1993).